



Treball Final de Grau

Structure-sensitive hydrogenation of NO using metal electrocatalysts

María Fernanda Lezana Muralles

June 2022



UNIVERSITAT DE
BARCELONA

Aquesta obra està subjecta a la llicència de:
Reconeixement–NoComercial–SenseObraDerivada



<http://creativecommons.org/licenses/by-nc-nd/3.0/es/>

Todos los triunfos nacen cuando nos atrevemos a comenzar

Eugene Ware

Quiero agradecer y dedicar este trabajo de fin de grado especialmente a mis papás y hermanos que, a pesar de la distancia, su apoyo, amor, confianza y motivación incondicional se sienten tan cerca como siempre y sin ellos, este logro no hubiese sido posible. Agradecer también a mis tíos, primos y abuelos (QEPD) que han estado siempre presentes en mi vida.

Gracias a las amistades y personas que he conocido tanto de Guatemala como de Barcelona, a los amigos que van y vienen y a los que se han quedado y se han convertido en la familia que uno escoge.

Y, por último, gracias a mi tutor, Dr. Federico Calle Vallejo, por aceptar ser mi tutor, enseñarme y guiarme en este proyecto, y a la estudiante de doctorado Eleonora Romeo por su ayuda en el último trayecto de este trabajo.

CONTENTS

SUMMARY	I
RESUMEN	III
IDENTIFICATION AND REFLECTION ON THE SUSTAINABLE DEVELOPMENT GOALS	V
1. INTRODUCTION	1
2. OBJECTIVES	3
3. THEORETICAL BACKGROUND	5
3.1 DFT: DENSITY FUNCTIONAL THEORY	5
3.2 VASP: VIENNA AB INITIO SIMULATION PACKAGE	9
3.3 BASIC THERMODYNAMICS	11
4. RESULTS	12
4.1 ADSORPTION SITES	12
4.2 ELECTROCHEMICAL HYDROGENATION OF *NO	18
4.3 SCALING RELATIONS	20
5. CONCLUSIONS AND OUTLOOK	25
REFERENCES AND NOTES	27
APPENDICES	31
APPENDIX 1: DATA IN CHAPTER 4	33

SUMMARY

The purpose of this thesis is to determine the most stable product of NO hydrogenation on a series of transition metal catalysts with sites of different surface coordination. Since it is unclear whether the first hydrogenated intermediate of NO electroreduction is $^*\text{NOH}$ or $^*\text{NHO}$, this work will show the adsorption energies at 6 different active sites of 9 transition metals (Co, Ni, Cu, Rh, Pd, Ag, Ir, Pt, and Au). To do so, density functional theory (DFT) calculations were carried out using the VASP code and the adsorption energies were calculated by means of the computational hydrogen electrode. Once the adsorption energies are calculated, this work is divided into three parts: the first one shows the most favorable adsorption sites of $^*\text{NO}$, $^*\text{NOH}$ and $^*\text{NHO}$ on each metal and surface site. The second part presents the findings from a thermodynamic perspective and with structural sensitivity of the most favorable product of $^*\text{NO}$ hydrogenation on transition metals. In the last part, universal adsorption-energy scaling relations are established among $^*\text{NO}$, $^*\text{NOH}$ and $^*\text{NHO}$.

Keywords: Nitric oxide, electrocatalysis, hydrogenation, structural sensitivity, density functional theory.

RESUMEN

El objetivo de este Trabajo Final de Grado (TFG) es determinar el producto más favorable de la hidrogenación de NO en una serie de catalizadores de metales de transición en sitios de diferente coordinación superficial. Dado que no está claro si el siguiente intermediario de la electrorreducción de *NO es *NOH o *NHO, en este trabajo se mostrarán las energías de adsorción en 6 sitios activos diferentes de 9 metales de transición (Co, Ni, Cu, Rh, Pd, Ag, Ir, Pt y Au). Para el análisis, se realizaron cálculos empleando la teoría del funcional de la densidad (Density Functional Theory/DFT) utilizando el código VASP, y las energías de adsorción se calcularon mediante el electrodo de hidrógeno computacional. Una vez calculadas las energías de adsorción, este trabajo se divide en tres partes: la primera muestra los sitios de adsorción más favorables de *NO, *NOH y *NHO en cada metal y sitio superficial. La segunda parte presenta los hallazgos desde una perspectiva termodinámica y con sensibilidad estructural del producto más favorable de hidrogenación de *NO sobre metales de transición. En la última parte se establecen relaciones universales de escala entre las energías de adsorción de *NO, *NOH y *NHO.

Palabras Clave: Óxido nítrico, electrocatálisis, hidrogenación, sensibilidad estructural, teoría del funcional de la densidad

IDENTIFICATION AND REFLECTION ON THE SUSTAINABLE DEVELOPMENT GOALS

The Sustainable Development Goals (SDGs), also known as Global Goals, are a universal call to action to eradicate poverty, safeguard the environment, and ensure that everyone lives in peace and prosperity by 2030. There are 17 goals that can be grouped into 5 major categories better known as “The 5Ps”, which are related to each other to work on specific challenges and know what actions to take.

It is important to understand how this project has an impact on the SDGs. We will focus on the following areas and goals: **Main area 1:** People (**Goal number 6:** Clean water and sanitation) and **Main area 2:** Planet (**Goal number 12:** Responsible consumption and production, **goal number 13:** Climate action, **goal number 14:** Life below water and **goal number 15:** Life on land).

We focus on these areas since, as we know, human activities such as the use of fertilizers, burning of fossil fuels, power generation plants and industry are causing a high increase in the amount of nitrogen exchanged between living organisms, the soil, water, and the atmosphere thus causing serious alterations in the nitrogen cycle. The imbalance of the nitrogen cycle has a negative impact on the formation of photochemical smog, loss of nutrients in the soil and acidification, loss of biological diversity and causing changes in plants and animals' life both on land and water. For this reason, one of the main objectives of this work is to know the most favorable product of the first hydrogenation step of NO on several catalysts, which contributes

positively to the development of the SDGs [1], as the electrochemical reduction of NO is an appealing option to balance the nitrogen cycle.

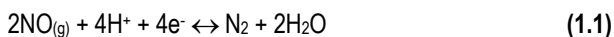
1. INTRODUCTION

The concept of planetary boundaries, introduced in 2009, can be defined as the Earth system limits where humanity can safely develop. There are nine planetary boundaries related to the Earth's biophysical systems and processes. If these limits are exceeded, many irreparable consequences will put human development in danger [2].

One of the most important planetary boundaries is related to the human interference with the nitrogen cycle, even though the public opinion tends to be unaware of it and is mostly focused on the problems related to the carbon cycle. Nowadays, human activities such as different modern forms of agriculture and the production and use of large amounts of fertilizers have caused a tremendous imbalance in the biogeochemical cycle of nitrogen. This has resulted in the transgression of the environmental boundary of nitrogen and the deleterious accumulation of nitrate and nitrite ions in groundwater.

Basically, the imbalance in the biogeochemical cycle of nitrogen can be understood as the presence of additional reactive nitrogen in the environment perturbing the global cycle of this important element. A way of easing such imbalance is by reducing nitrate to dinitrogen or ammonia. This can be done by the electrochemical reduction of oxidized nitrogen species, such as nitrate, nitrite and NO.

Nitrate can be reduced first to nitrite and then to NO. In turn, NO can be reduced to N₂ via this reaction in acid media[3]:



The first step in NO reduction is NO adsorption. Then, *NO is electrochemically hydrogenated to either *NOH or *NHO following these reactions:



NO adsorption and reactivity on metal surfaces are considered of great interest for technological and scientific purposes [3], as only by elucidating the reaction mechanism can NO reduction electrocatalysts be rationally optimized. In this work, we evaluated the most thermodynamically stable product of *NO hydrogenation depending on the transition metal catalyst and the coordination number of the active sites. We evaluated 9 different transition metals (Co, Ni, Cu, Rh, Pd, Ag, Ir, Pt, and Au) and 6 different active sites.

2. OBJECTIVES

The main objectives of this work were:

- To determine the most favorable adsorption sites of *NO, *NOH and *NHO depending on the transition metal and surface facet.
- To find from a thermodynamic perspective and with structural sensitivity, the most favorable product of the hydrogenation of *NO on transition metals.
- To establish adsorption-energy scaling relations among *NO, *NOH and *NHO.

To accomplish these objectives, 6 surface facets of 9 different transition metals were analyzed using DFT calculations. The following were the tasks carried out to achieve those goals:

- Determine the total energy of the clean surfaces with DFT.
- Determine the most stable configurations of the surfaces with *NO, *NOH and *NHO and their corresponding total energies.
- Determine the total energy of NO(g) and H₂(g).
- Assess the zero-point energies, TS corrections and solvation corrections.
- With the aforementioned data calculate the free energies of adsorption of *NO, *NOH and *NHO for the different surface facets.
- Analyze the trends through adsorption-energy scaling relationships between the reaction intermediates.
- Elaborate a matrix showing the most stable product of *NO hydrogenation according to the metal and active site.

3. THEORETICAL BACKGROUND

3.1 DFT: DENSITY FUNCTIONAL THEORY

The description of the structure and dynamics of different electron systems is one of the central problems of theoretical chemistry. These systems may be composed of single atoms, molecules of all kinds, clusters, quantum dots and solids organized in layers, surfaces, and quasi-crystals [4]. Electronic structure plays a key role in determining the stability of the system, many of its thermodynamic properties and in transport properties such as electrical conductivity, among others.

In this context, an interesting matter is how the energy varies as a function of the movement of atoms. First, it is important to define where the nuclei and the electrons are. Electrons react to changes in their surroundings far faster than the nuclei because atomic nuclei are considerably heavier and slower than the electrons, so their motion can be considered separately. For fixed positions of atomic nuclei, the resolution of equations that describe the electron mobility is possible. Then, it is also possible to find the lowest-energy configuration also known as ground-state for a given set of electrons moving around a set of nuclei. This function is called the adiabatic potential energy surface of the atoms and the decoupling of the equations is known as the Born-Oppenheimer approximation.

Since the 1990s Density Functional Theory (DFT) has become the standard tool for modeling materials at the atomic scale in chemistry, chemical engineering, surface science and catalysis, as it is an easy-to-solve approach for the description of many-body systems. DFT calculations provide information that can be correlated to experiments, and sometimes it even gives access to information that is unobtainable through experiments.

To get an idea of what DFT is about, it is helpful to understand its connection to quantum mechanics. In quantum mechanics, particles can act as classical waves. Thus, all the information of a given system is contained in the wavefunction of the system, which is determined using the stationary form with N electrons of the Schrödinger equation:

$$H\psi = E\psi \quad (3.1)$$

Where H is the Hamiltonian operator, E is a constant equal to ground-state energy and is in this case independent of time, and ψ is the electronic wavefunction or set of solutions of the Hamiltonian, which depends on the spatial coordinates of each electron. The solution we are interested in is the one that describes the interaction between multiple electrons with multiple nuclei. To simplify the calculations, the Born-Oppenheimer approximation is used because it divides nuclei and electrons into separate mathematical problems. If there is more than one electron, the time-independent Schrödinger equation is:

$$\left[-\frac{\hbar^2}{2m} \sum_{i=1}^N \nabla_i^2 + \sum_{i=1}^N V(r_i) + \sum_{i=1}^N \sum_{i < j} U(r_i, r_j) \right] \psi = E\psi \quad (3.2)$$

In **Equation 3.2**, \hbar is the reduced Planck constant, m is the electron mass, ∇^2 is the Laplacian operator and the three terms inside the brackets are in order: the kinetic energy of each electron, the interaction energy between every single electron and the set of atomic nuclei and the interaction energy between different electrons.

As all the information of the system is gathered in the wavefunction, this can be approximate as a product of individual electron wavefunctions and the previous equation must be solved with different approximations, such that the Schrödinger equation is a many-body problem.

The Hartree product is one of the most basic methods for approximating a solution. The full wave of a single molecule is determined by the number of electrons, in each of the spatial coordinates (x, y, z) even though this information cannot be directly observed.

Alternatively, the electron density, abbreviated as $n(\mathbf{r})$, describes the information that can be physically observable in terms of the 3 coordinates, expressed as:

$$n(\mathbf{r}) = 2 \sum_i \psi_i^*(\mathbf{r}) \psi_i(\mathbf{r}) \quad (3.3)$$

The product inside the summation is the probability that an electron is located at position (\mathbf{r}). The factor 2 is there because electrons have spin and according to the Pauli exclusion principle, two separate electrons can only occupy the same orbital if they have different spins [4], [5].

The foundations of DFT are in the Hohenberg-Kohn (HK) theorem which ensures that given a ground-state electron density, it is possible to calculate the corresponding ground-state wavefunction and its energy. As a result, the total-energy functional can be expressed as follows:

$$E[\{\psi_i\}] = E_{\text{known}}[\{\psi_i\}] + E_{\text{XC}}[\{\psi_i\}] \quad (3.4)$$

The previous equation is divided into two terms: $E_{\text{XC}}[\{\psi_i\}]$ which is the exchange-correlation functional and includes all the quantum mechanical effects not accounted by the other term, $E_{\text{known}}[\{\psi_i\}]$, which is defined:

$$E_{\text{known}}[\{\psi_i\}] = -\frac{\hbar^2}{2m} \sum_i \int \psi_i^* \nabla^2 \psi_i d^3\mathbf{r} + \int V(\mathbf{r})n(\mathbf{r})d^3\mathbf{r} + \frac{e^2}{2} \iint \frac{n(\mathbf{r})n(\mathbf{r}')}{|\mathbf{r} - \mathbf{r}'|} d^3\mathbf{r}d^3\mathbf{r}' + E_{\text{ion}} \quad (3.5)$$

The terms on the right-hand side represent, respectively, the electron kinetic energies and the Coulomb interactions between the electrons and the nuclei, electron pairs and nuclei pairs.

DFT can be implemented in different ways but one of the most efficient ones is the Kohn-Sham (KS) approach. The KS equations are a set of equations that can only be solved for single-electron wavefunctions based on the three spatial variables. These equations are similar the Schrödinger equation:

$$\left[-\frac{\hbar^2}{2m} \nabla^2 + V(r) + V_H(r) + V_{XC}(r) \right] \psi_i(r) = \varepsilon_i \psi_i(r) \quad (3.6)$$

Where the three terms represent different potentials: V is the interaction between one electron and the collection of atom nuclei, V_H is the Hartree potential that involves a Coulomb interaction between the electron and itself as part of the total electronic density:

$$V_H(r) = e^2 \int \frac{n(r')}{|r-r'|} d^3r' \quad (3.7)$$

and V_{XC} is a functional derivative of the exchange-correlation energy:

$$V_{xc}(r) = \frac{\delta E_{XC}(r)}{\delta n(r)} \quad (3.8)$$

It is necessary to employ an iterative algorithm to solve the KS equations. First, a starting electron density is assumed. Then, using **Equation 3.6**, the electron wavefunction is calculated. Third, the electron density using **Equation 3.3** is calculated and compared with the initial one. The ground-state density is said to be found if both results are the same or within a given tolerance. If they are not, the calculated electron density is used as a new starting point and the algorithm is restarted [5], [6].

3.2 VASP: VIENNA AB INITIO SIMULATION PACKAGE

The Vienna Ab initio Simulation Package (VASP) is a computer program that uses first-principles calculations to model materials at the atomic scale. VASP performs static or dynamic calculations by approximating a solution to the many-body Schrödinger equation with either DFT or the Hartree approximation [7]. In this thesis, the calculations were performed with DFT.

Before using VASP, it is necessary to learn the basic commands of Bash, which is the command-interpreter and programming language of Linux. Afterwards, the simulations and calculations can be sent to a computer cluster.

To carry out the calculations it is necessary to send five input files: POSCAR, INCAR, POTCAR, KPOINTS and a submission script. The POSCAR contains the periodic lattice, a set of spatial coordinates for sites in a unit cell and the atomic species symbols and their number. The POTCAR holds information about the atomic species, and their ordering must match that of the POSCAR file to prevent errors during the calculations. In this work, I used the projector augmented-wave (PAW) method [8], and the PBE exchange-correlation functional [9]. The KPOINTS file contains the k-point sampling used to solve differential equations in the Fourier space or k-space, and specifies its implementation: in this work, I used Monkhorst-Pack grids [10]. The INCAR file has information on the numerical methods: for instance, it contains a parameter called ENCUT (the plane-wave cutoff), which determines how precise the calculation will be; NSW sets a limit to the maximum number of iterations to carry out; POTIM specifies the step size during the optimization; EDIFF and EDIFFG are the convergence criteria for the electronic and ionic loops; and IBRION specifies the optimization algorithm (conjugate gradient, in this case). The submission script contains instructions for the computer cluster to execute VASP.

Once the calculations are done, the supercomputer returns the output files. Generally, I was interested in the OUTCAR and CONTCAR files. The former file has information about energy, electronic steps, stress tensors and some other useful information. The latter file provides the last spatial coordinates of the calculation, which correspond to the DFT ground state in case the calculation converged. If it did not, the CONTCAR can be used to start a new calculation.

3.3 BASIC THERMODYNAMICS

The Gibbs free energy (G) is the amount of energy accessible of a system and predicts how the system will behave. This quantity is the energy associated with a chemical reaction that can be used to do work, and it is the subtraction of the enthalpy (H) and the product of the temperature and the entropy (TS) of the system:

$$G = H - TS \quad (3.9)$$

For a chemical reaction, the change of free energy (ΔG) is defined as the difference between the free energy of products and reactants. At standard state conditions (298.15 K and 1 atm) we have [11]:

$$\Delta G^0 = \sum v \Delta_f G^0_{(\text{products})} - \sum v \Delta_f G^0_{(\text{reactants})} \quad (3.10)$$

The free energy of adsorption of a catalytic intermediate is obtained in this thesis from DFT calculations by means of the following equation:

$$\Delta G_{\text{ads}} = \Delta E_{\text{DFT}} + \Delta ZPE - T\Delta S + \Delta E_{\text{solvation}} \quad (3.11)$$

Where the first term on the right is the DFT-calculated adsorption energy of a specific intermediate, ΔZPE is the change in zero-point energy (calculated with DFT using the harmonic oscillator approximation), ΔS is the change of entropy and T is the absolute temperature in K. S was calculated at 298.15 K making use of the harmonic-oscillator approximation for adsorbates and taken from the literature for gases [12]. The last term contains solvation corrections in water depending on the chemical nature of the adsorbates and the values for *NO, *NOH and *NHO were taken from a previous work [13].

4. RESULTS

4.1 ADSORPTION SITES

A key issue in the electrochemical reduction of *NO is to elucidate the reaction intermediates. The hydrogenation of *NO leads either to *NOH or *NHO. The latter two adsorbates bind differently depending on the metal and the geometry of the adsorption sites. Apart from that, in this work we looked at trends in the adsorption energies of the adsorbates bound to various transition metal surfaces.

As shown in **Figures 4.1 and 4.2**, in this study we evaluated six different facets of nine transition metals (Co, Ni, Cu, Rh, Pd, Ag, Ir, Pt, Au). The facets are as follows: two different terraces, namely (111) and (100); edges at (211); kinks at (211k); three metal adatoms at a (111) terrace (3AD@111); and four adatoms at a (100) terrace (4AD@100). The coordination numbers (cn) span from 5 to 9: for (111) terraces, $cn = 9$; for (100) terraces, $cn = 8$; for (211) step edges, $cn = 7$; for kink sites at 211k, $cn = 6$; for the adatoms at 4AD@100, $cn = 6$; and for the adatoms at 3AD@111, $cn = 5$. We cover such a wide range of coordination numbers in an attempt to typify the heterogeneity of a real catalyst [14]. On each transition metal site *NO, *NOH and *NHO were fully relaxed over several adsorption sites and configurations. We inspected monodentate configurations for *NO, *NOH and *NHO (top, bridge, and hollows, see **Figure 4.1**) and bidentate configurations only for *NHO (bridge-top, bridge-bridge, top-top and diagonal, see **Figure 4.2**).

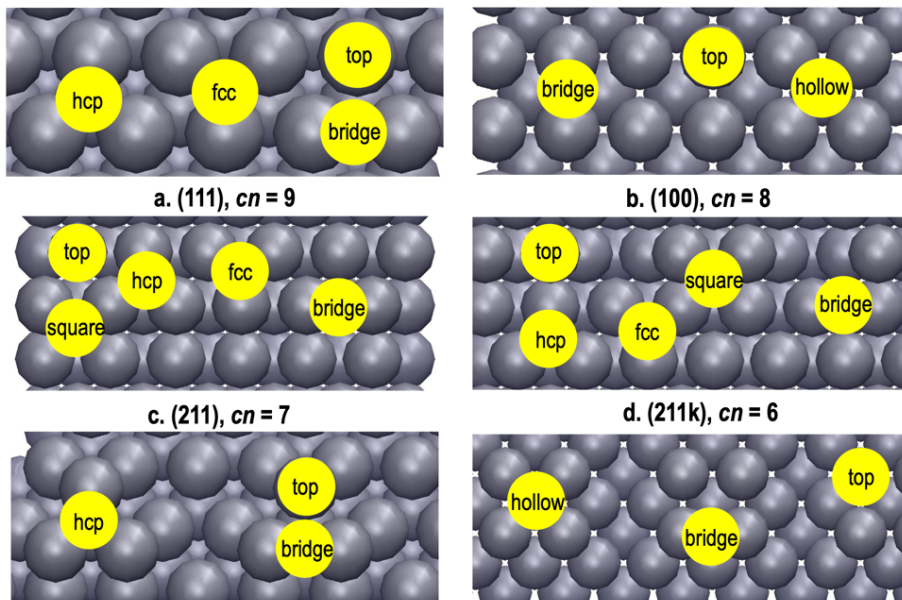


Figure 4.1. Active sites on fcc transition metals for the monodentate adsorption of *NO, *NOH and *NHO.

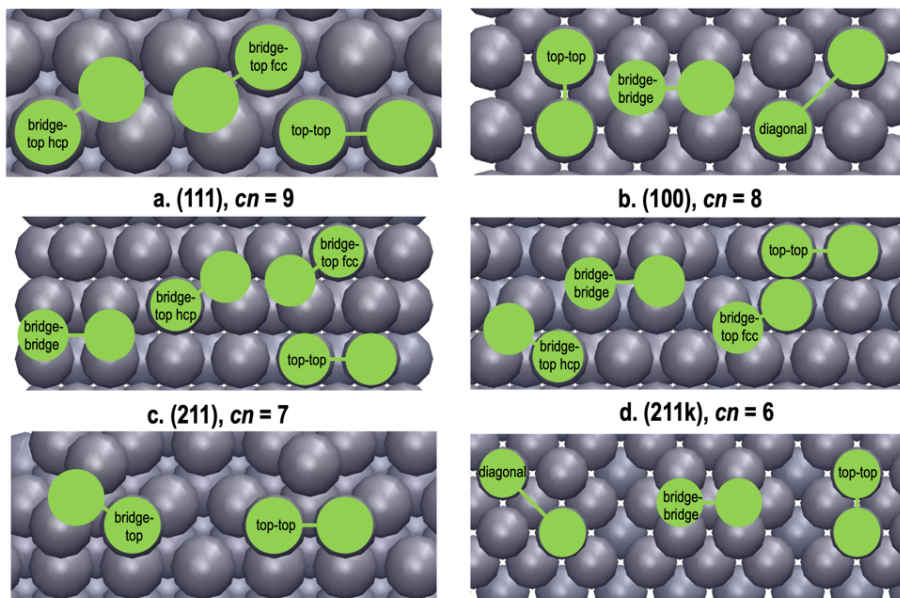


Figure 4.2. Active sites on fcc transition metals for the bidentate adsorption of $*\text{NHO}$. Top-top: both O and N bind atop. Bridge-bridge: both O and N bind to bridge sites. Bridge-top: N binds on the bridge and O on top or vice versa. This adsorption configuration can take place over fcc or hcp hollows.

By comparing the adsorption energies calculated with DFT and making use of the computational hydrogen electrode [15], we can analyze in a simple and quantitative way the most stable adsorption sites per adsorbate, metal, and facet for $*\text{NO}$, $*\text{NOH}$ and $*\text{NHO}$. The nine transition metals analyzed here belong to groups 9 (Co, Rh, Ir), 10 (Ni, Pd, Pt) and 11 (Cu, Ag, Au) of the periodic table. The d-bands of the metals tend to contain more electrons as the group number increases. This is important to note because the features of the d-bands give rise to properties that are of great importance during catalytic and electrocatalytic reactions [16]–[18].

In addition, differences or similarities can be observed among the transition metals belonging to a given period of the periodic table. In this case, we can group the nine transition metals as follows: 3d series (Co, Ni, Cu), 4d series (Rh, Pd, Ag), and 5d series (Ir, Pt, Au). **Tables 4.1-4.3** contain the most stable adsorption sites per metal, and facet for *NO, *NOH and *NHO.

In **Table 4.1**, we observe for the 3d series a tendency to bind *NO at hollow sites, in particular hcp sites. The main exception is the 4AD@100 facet (bridge site for the three metals). When comparing the metals in the 4d series, Rh adsorbs over bridge and hollow sites, while Pd and Ag tend to prefer hollow sites. For the 5d series, the most stable site is either bridge or hollow for highly coordinated facets, whereas it is either top or bridge for undercoordinated facets. Statistically, we can say that 54% of the times *NO adsorbs on a hollow, 35% on a bridge site and 11% on a top site (corresponding to 5d metals with $cn \leq 6$).

Table 4.1. Most stable adsorption sites per metal and facet for *NO.

metal	111 $cn = 9$	100 $cn = 8$	211 $cn = 7$	211k $cn = 6$	4AD @ 100 $cn = 6$	3AD @ 111 $cn = 5$
Co	hcp	hollow	bridge	bridge	bridge	hcp
Ni	hcp	hollow	hcp	hcp	bridge	hcp
Cu	fcc	hollow	hcp	hcp	hollow	hcp
Rh	hcp	bridge	bridge	bridge	bridge	hcp
Pd	fcc	hollow	hcp	hcp	bridge	hcp
Ag	fcc	hollow	bridge	hcp	hollow	hcp
Ir	hcp	bridge	bridge	top	top	top
Pt	fcc	bridge	bridge	bridge	bridge	top
Au	fcc	bridge	bridge	top	bridge	top

Table 4.2 shows that the most stable adsorption sites for *NOH are hollows. On the (111) facet, *NOH typically prefers to adsorb on fcc hollows, whereas it prefers hcp hollows on the other facets. In addition, adsorption at bridges is only observed on 5d metals, namely, Ir, Pt and Au. According to statistics, we can say that 87% of the times *NOH adsorbs on a hollow, be it square, fcc or hcp, and 13% of the times *NOH adsorbs on a bridge site on a 5d metal surface. In no case is *NOH adsorbed on top sites.

Table 4.2. Most stable adsorption sites per metal and facet for *NOH.

metal	111 <i>cn</i> = 9	100 <i>cn</i> = 8	211 <i>cn</i> = 7	211k <i>cn</i> = 6	4AD @ 100 <i>cn</i> = 6	3AD @ 111 <i>cn</i> = 5
Co	hcp	hollow	hcp	hcp	hollow	hcp
Ni	fcc	hollow	hcp	fcc	hollow	hcp
Cu	fcc	hollow	hcp	fcc	hollow	hcp
Rh	hcp	hollow	hcp	hcp	hollow	hcp
Pd	fcc	hollow	fcc	fcc	hollow	hcp
Ag	fcc	hollow	square	square	hollow	hcp
Ir	fcc	bridge	bridge	bridge	hollow	hcp
Pt	fcc	bridge	fcc	bridge	bridge	hcp
Au	fcc	hollow	bridge	fcc	bridge	hcp

As mentioned at the beginning of this section, *NHO can be adsorbed in two different configurations: monodentate (via N-metal bonds) and bidentate (via N-metal and O-metal bonds). According to **Table 4.3**, *NHO generally adsorbs in a bidentate fashion (93% of the cases, mostly Nbr-Otop and br-br and top-top configurations). On the (111) surface the most common adsorption configuration is with N adsorbed on the bridge and O on top (Nbr-Otop). Bridge-bridge is the most common site on the (100) surface. On the (211) and (211k) facets the most common adsorption site is top-top or N on bridge and O on top. On 4AD@100 the most favorable adsorption site is generally found at br-br sites, whereas Nbr-Otop is most favorable on 3AD@111.

Table 4.3. Most stable adsorption sites per metal and facet for *NHO.

metal	111 cn = 9	100 cn = 8	211 cn = 7	211k cn = 6	4AD @ 100 cn = 6	3AD @ 111 cn = 5
Co	Nbr-Otop hcp	br-br	br-br	Nbr-Otop hcp	br-br	Nbr-Otop
Ni	Nbr-Otop fcc	br-br	Nbr-Otop hcp	Nbr-Otop hcp	br-br	Nbr-Otop
Cu	Nbr-Otop hcp	br-br	br-br	top-top	br-br	Nbr-Otop
Rh	Nbr-Otop hcp	br-br	top-top	top-top	br-br	Nbr-Otop
Pd	Nbr-Otop fcc	br-br	top-top	Nbr-Otop fcc	br-br	Nbr-Otop
Ag	Nbr-Otop hcp	br-br	top-top	top-top	top-top	Nbr-Otop
Ir	Nbr-Otop hcp	top- top	top-top	top-top	br-br	Nbr-Otop
Pt	Nbr-Otop fcc	br-br	top-top	top-top	top-top	Nbr-Otop
Au	top	bridge	bridge	top-top	top-top	top

4.2 ELECTROCHEMICAL HYDROGENATION OF *NO

Table 4.4 illustrates the most favorable product of the hydrogenation of *NO on transition metals (see **Equations 1.3-1.4** from section 1). We observe that the most common adsorbed product of *NO hydrogenation is *NHO, which represents 69% of the total, while *NOH dominates in 19% of the surface sites and in 13% for cases the difference of the two intermediates is smaller than 0.1 eV. Analyzing each facet, we conclude that square facets, namely (100) and (4AD@100) preferentially form *NHO on most transition metals, and *NOH is common only on the (111) facet.

Table 4.4. Most stable adsorbates formed upon the first hydrogenation of *NO.¹

metal	111 <i>cn</i> = 9	100 <i>cn</i> = 8	211 <i>cn</i> = 7	211k <i>cn</i> = 6	4AD @ 100 <i>cn</i> = 6	3AD @ 111 <i>cn</i> = 5
Co	NOH	NHO	both	both	NHO	NHO
Ni	NOH	NHO	NOH	NOH	NHO	both
Cu	NOH	NHO	NHO	NHO	NHO	NHO
Rh	NOH	NHO	both	NHO	NHO	NHO
Pd	NOH	NHO	both	NOH	NHO	both
Ag	NHO	NHO	NHO	NHO	NHO	NHO
Ir	NOH	NHO	NHO	NHO	NHO	NHO
Pt	NOH	NHO	NHO	NHO	NHO	both
Au	NHO	NHO	NHO	NHO	NHO	NHO

¹ In case the absolute difference between the adsorption energies of *NHO and *NOH is less than 0.1 eV, both intermediates are reported.

Except for gold and silver, which selectively form *NHO , transition metals are not entirely selective toward *NOH or *NHO . Ir and Cu are also rather selective toward *NHO , as all of their sites form *NHO except for the (111) facet. In general, elements in the 5d series are more selective than those in the 3d and 4d series, and elements with more d electrons also tend to be more selective.

4.3 SCALING RELATIONS

Figure 4.3 was created using the most stable adsorption energies of the three intermediates in each of the nine metals and facets. The result is a set of graphs that demonstrates the universality of the scaling relations between the adsorption energies of *NO and *NHO (red squares) and *NO and *NOH (blue triangles). This means that the three sets of adsorption energies are linearly related regardless of the coordination of the adsorption sites.

Now, if we carefully analyze the slopes of the lines for *NOH vs *NO and *NHO vs *NO, we see that the average of the slope does not strongly depend on the coordination number, see **Figure 4.4**. For *NOH vs *NO, $m \approx 1.02 \pm 0.06$. Similarly, for *NHO vs *NO, $m \approx 0.92 \pm 0.10$. These values indicate that the binding of *NOH, *NHO and *NO is, electronically speaking, nearly identical [19].

The data in the separate panels of **Figure 4.3** have been brought together in **Figure 4.5**. This figure provides the overall trends of the adsorption energies of the intermediates for all the nine metals and six facets. In line with *CHO vs *CO trends (see Figure 4 in reference [14]), a single line describes the trends in adsorption energies for *NHO vs *NO across all facets. However, for *COH vs *CO it was observed that sites with different coordination numbers required separate lines, whereas in this case, a single line in **Figure 4.5** represents the trends for *NOH vs *NO.

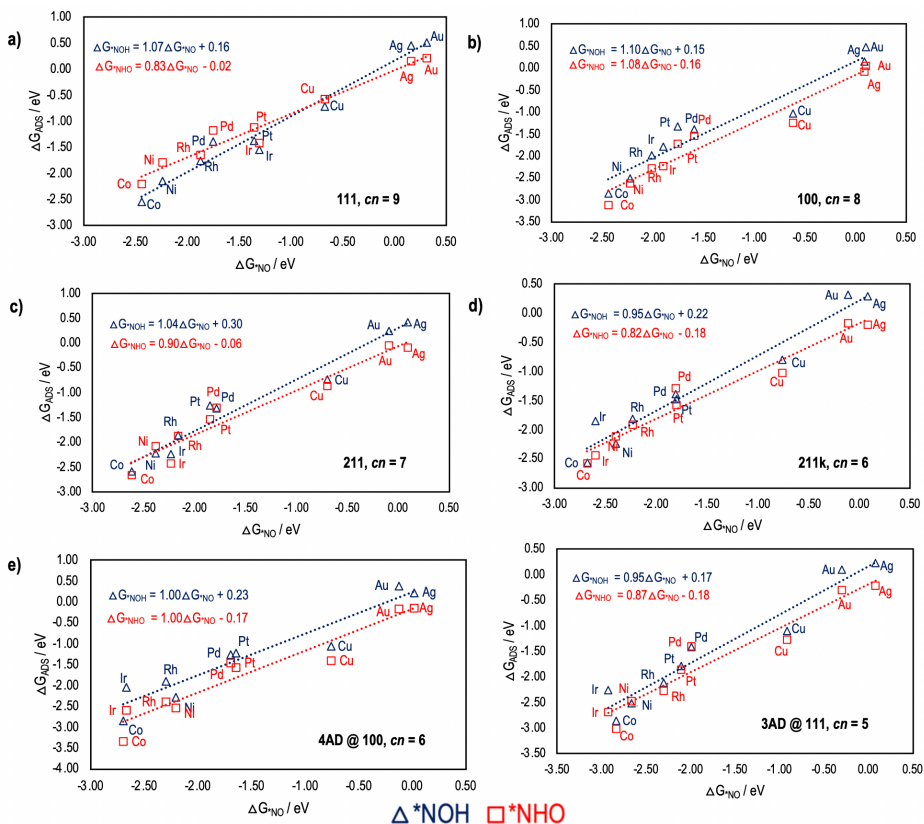


Figure 4.3. Adsorption-energy scaling relations between ΔG^*_{NO} , ΔG^*_{NOH} and ΔG^*_{NHO} . Each panel contains the most stable adsorption energies of the nine metals under study for the three intermediates. The equations of the linear fits are provided in each case.

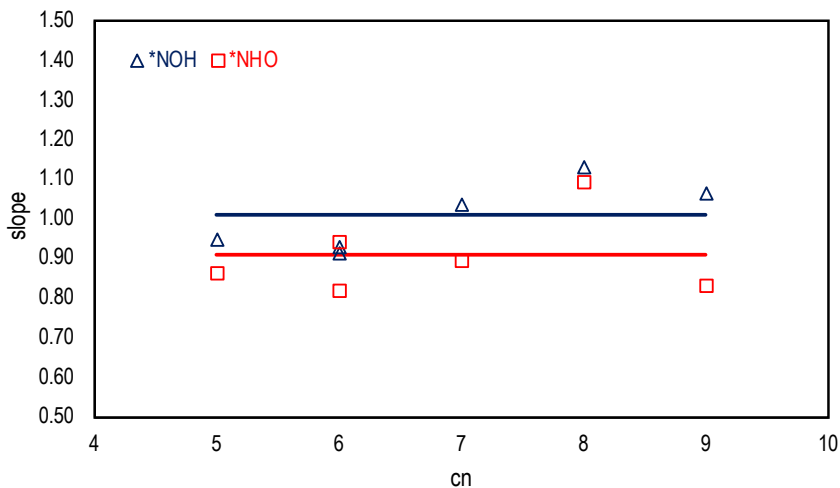


Figure 4.4. Structure sensitivity of the slope of the scaling relations between ΔG^{*NOH} vs ΔG^{*NO} (blue) and ΔG^{*NHO} vs ΔG^{*NO} (red). The slopes are relatively independent of the coordination number of the adsorption sites. The blue and red lines mark the average values of the slopes.

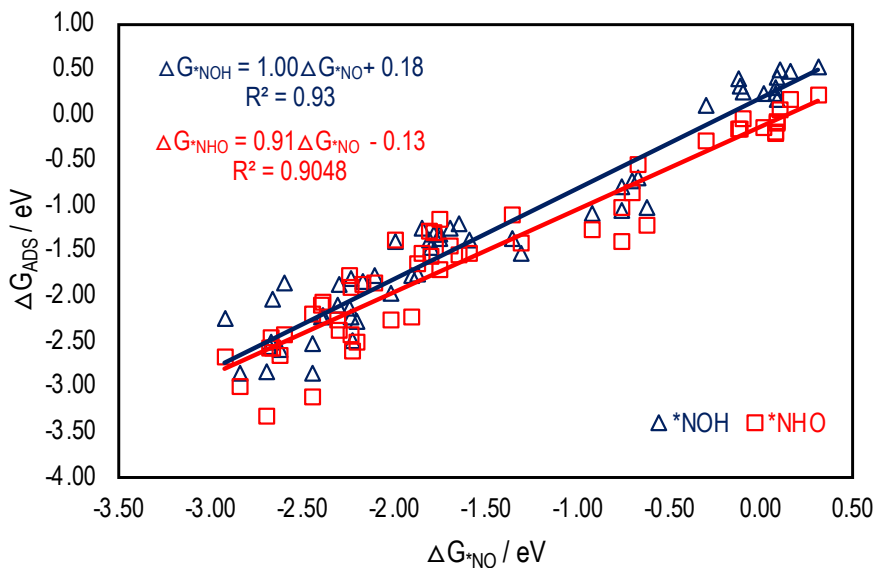


Figure 4.5. Universal adsorption-energy scaling relations for ΔG^{*NOH} vs ΔG^{*NO} (blue) and ΔG^{*NHO} vs ΔG^{*NO} (red) for nine transition metals on six different surface facets.

5. CONCLUSIONS AND OUTLOOK

The goal of this study was to find from a thermodynamic perspective and with structural sensitivity the most favorable product of the electrochemical hydrogenation of *NO on nine late transition metals. The following conclusions can be drawn from the results presented in Chapter 4.

- For *NO and *NOH there is the tendency to adsorb on hollow sites while *NHO tends to bind over 3 different bidentate sites (Nbr-Otop, br-br and top-top).
- The most stable product of the hydrogenation of *NO on transition metals is generally *NHO. There are also some cases where both intermediates are nearly equally stable.
- The square facets (i.e., (100) and (4AD@100)) selectively form *NHO on the nine transition metals. In turn, *NOH is common only on the (111) facet except for silver and gold.
- The scaling relations between the adsorption energies of *NO, *NHO and *NOH are universal. In other words, those three adsorbates are linearly related regardless of the coordination of the adsorption sites.
- The values of the slopes for *NOH vs *NO and *NHO vs *NO indicate that the binding of the intermediates is, electronically speaking, nearly identical.
- Solvation corrections from previous works calculated for Pt(111) were used for all metals and facets. The conclusions might change if the solvation corrections were calculated for every metal. This can be inspected in future works.

REFERENCES AND NOTES

- [1] United Nations, "Take Action for the Sustainable Development Goals." <https://www.un.org/sustainabledevelopment/development-agenda/> (accessed May 05, 2022).
- [2] J. , Rockström et al., "A safe operating space for humanity," vol. 461, 2009, doi: 10.1038/461472a.
- [3] V. Rosca, M. Duca, M. T. de Groot, and M. T. M. Koper, "Nitrogen Cycle Electrocatalysis." *Chemical Reviews*, vol. 109, no. 6, pp. 2209–2244, Jun. 2009, doi: 10.1021/cr8003696.
- [4] E. Engel and R. M. Dreizler, *Density Functional Theory: An Advanced Course*. Berlin, Heidelberg: Springer Berlin Heidelberg, 2011. doi: 10.1007/978-3-642-14090-7.
- [5] D. S. Sholl and J. A. Steckel, *DENSITY FUNCTIONAL THEORY A Practical Introduction*. New Jersey: John Wiley & Sons, 2009.
- [6] K. Capelle, "A Bird's-Eye View of Density-Functional Theory," *Brazilian Journal of Physics*, vol. 36, no. 4A, 2006, doi: 10.1590/S0103- 97332006000700035.
- [7] G. , Kresse and J. Furthmüller, "Efficiency of ab-initio total energy calculations for metals and semiconductors using a plane-wave basis set," 1996. doi: 10.1016/0927-0256(96)00008-0.
- [8] G. Kresse and D. Joubert, "From ultrasoft pseudopotentials to the projector augmented-wave method," 1999. doi: 10.1103/PhysRevB.59.1758.
- [9] J. P. Perdew, K. Burke, and M. Ernzerhof, "Generalized Gradient Approximation Made Simple," *Physical Review Letters*, vol. 77, no. 18, pp. 3865–3868, Oct. 1996, doi: 10.1103/PhysRevLett.77.3865.
- [10] H. J. Monkhorst and J. D. Pack, "Special points for Brillouin-zone integrations," *Physical Review B*, vol. 13, no. 12, pp. 5188–5192, Jun. 1976, doi: 10.1103/PhysRevB.13.5188.
- [11] R. , Chang and Zimmerman, *Physical chemistry for the biosciences*, vol. 33. Sausalito: University Science Books, 2005. doi: 10.1002/bmb.2005.49403305383.
- [12] D. R. Lide et al., *CRC Handbook of Chemistry and Physics Editor-in-Chief*, 85th ed. CRC Press, 2005. doi: 10.1021/ja041017a.
- [13] A. Clayborne, H.-J. Chun, R. B. Rankin, and J. Greeley, "Elucidation of Pathways for NO Electroreduction on Pt(111) from First Principles," *Angewandte Chemie International Edition*, vol. 54, no. 28, pp. 8255–8258, Jul. 2015, doi: 10.1002/anie.201502104.
- [14] F. Calle-Vallejo and M. T. M. Koper, "Accounting for bifurcating pathways in the screening for CO₂ reduction catalysts," *ACS Catalysis*, vol. 7, no. 10. American Chemical Society, pp. 7346–7351, Oct. 06, 2017. doi: 10.1021/acscatal.7b02917.

- [15] J. K. Nørskov et al., “Origin of the Overpotential for Oxygen Reduction at a Fuel-Cell Cathode,” *The Journal of Physical Chemistry B*, vol. 108, no. 46, pp. 17886–17892, Nov. 2004, doi: 10.1021/jp047349j.
- [16] B. Hammer and J. K. Nørskov, “Theoretical surface science and catalysis—calculations and concepts,” 2000, pp. 71–129. doi: 10.1016/S0360-0564(02)45013-4.
- [17] J. K. Nørskov, T. Bligaard, J. Rossmeisl, and C. H. Christensen, “Towards the computational design of solid catalysts,” *Nature Chemistry*, vol. 1, no. 1, pp. 37–46, Apr. 2009, doi: 10.1038/nchem.121.
- [18] F. Calle-Vallejo et al., “Number of outer electrons as descriptor for adsorption processes on transition metals and their oxides,” *Chemical Science*, vol. 4, no. 3, p. 1245, 2013, doi: 10.1039/c2sc21601a.
- [19] F. Calle-Vallejo, J. I. Martínez, J. M. García-Lastra, J. Rossmeisl, and M. T. M. Koper, “Physical and Chemical Nature of the Scaling Relations between Adsorption Energies of Atoms on Metal Surfaces,” *Physical Review Letters*, vol. 108, no. 11, p. 116103, Mar. 2012, doi: 10.1103/PhysRevLett.108.116103.
- [20] R. Urrego-Ortiz, S. Builes, and F. Calle-Vallejo, “Fast Correction of Errors in the DFT-Calculated Energies of Gaseous Nitrogen-Containing Species,” *ChemCatChem*, vol. 13, no. 10, pp. 2508–2516, May 2021, doi: 10.1002/cctc.202100125.

APPENDICES

APPENDIX 1: DATA IN CHAPTER 4

To compute the tables in Section 3.1 it is necessary to know the adsorption energies of the molecules, the zero-point energy corrections (ZPE), the solvation energies, the entropy corrections (TS at $T = 298.15$ K) and the Gibbs energy (G) to determine the most stable adsorption site for each metal and facet [12], [13].

Table A1 contains the ZPE and TS for H_2 and NO. Following previous works, the gas phase of NO was corrected by -0.07 eV [20] **Table A2** shows the average ZPE and product TS_{vib} for the adsorbed species on each facet. Finally, **Table A3** contains the most stable adsorption energies for each metal and facet.

To compute **Table 4.4** from Section 3.2, it is necessary to calculate the free energy of adsorption (ΔG) of each intermediate (available in **Table A3.**) following **Equation 2.11** from Chapter 2. These data are also useful to build **Figure 4.3** and **Figure 4.5** in Section 4.3. Besides, **Table A4** provides the differences between the adsorption energies of *NHO and *NOH. To build **Figure 4.4** in Section 4.3 data from **Table A5** were used. The solvation corrections used in this study were: 0, -0.31 and -0.23 eV for *NO, *NOH and *NHO, taken from previous works [13].

Table A1. ZPE energy, entropy corrections and gas-phase correction (from ref. [20]) for the gases in this study.

Species	ZPE [eV]	TS [eV]	Gas-phase correction [eV]
NO	0.12	0.65	-0.07
H ₂	0.27	0.40	0.00

Table A2. Average ZPE and TS_{vib} for the adsorbed species on each facet.

111		
adsorbed species	ZPE [eV]	TS_{vib} [eV]
*NO	0.18	0.13
*NOH	0.44	0.16
*NHO	0.47	0.12
100		
*NO	0.17	0.14
*NOH	0.44	0.16
*NHO	0.47	0.10
211		
*NO	0.18	0.14
*NOH	0.46	0.14
*NHO	0.47	0.13
211k		
*NO	0.21	0.14
*NOH	0.45	0.15
*NHO	0.47	0.13
4AD @ 100		
*NO	0.17	0.13
*NOH	0.44	0.15
*NHO	0.46	0.12
3AD @ 111		
*NO	0.18	0.13
*NOH	0.47	0.14
*NHO	0.47	0.12

Table A3. Free energies of adsorption per metal and facet for *NO, *NOH and *NHO.

facet	metal	ΔG^{*NO} [eV]	ΔG^{*NOH} [eV]	ΔG^{*NHO} [eV]
111	Co	-2.44	-2.54	-2.20
	Ni	-2.24	-2.15	-1.78
	Cu	-0.67	-0.70	-0.56
	Rh	-1.87	-1.76	-1.65
	Pd	-1.75	-1.38	-1.16
	Ag	0.16	0.46	0.16
	Ir	-1.30	-1.53	-1.42
	Pt	-1.36	-1.37	-1.11
	Au	0.31	0.52	0.21
100	Co	-2.44	-2.85	-3.11
	Ni	-2.22	-2.50	-2.61
	Cu	-0.62	-1.03	-1.23
	Rh	-2.01	-1.98	-2.27
	Pd	-1.59	-1.40	-1.54
	Ag	0.08	0.16	-0.08
	Ir	-1.90	-1.78	-2.23
	Pt	-1.75	-1.32	-1.71
	Au	0.10	0.48	0.05
211	Co	-2.62	-2.60	-2.66
	Ni	-2.39	-2.23	-2.08
	Cu	-0.70	-0.74	-0.87
	Rh	-2.17	-1.85	-1.88
	Pd	-1.78	-1.33	-1.30
	Ag	0.09	0.41	-0.10
	Ir	-2.23	-2.24	-2.44
	Pt	-1.85	-1.26	-1.54
	Au	-0.09	0.24	-0.05

211k	Co	-2.68	-2.57	-2.58
	Ni	-2.40	-2.25	-2.12
	Cu	-0.76	-0.81	-1.03
	Rh	-2.23	-1.82	-1.92
	Pd	-1.81	-1.40	-1.29
	Ag	0.08	0.29	-0.19
	Ir	-2.60	-1.86	-2.44
	Pt	-1.80	-1.47	-1.58
	Au	-0.11	0.31	-0.17
4AD @ 100	Co	-2.69	-2.84	-3.34
	Ni	-2.20	-2.28	-2.52
	Cu	-0.76	-1.06	-1.40
	Rh	-2.30	-1.88	-2.39
	Pd	-1.69	-1.25	-1.45
	Ag	0.02	0.23	-0.15
	Ir	-2.66	-2.04	-2.58
	Pt	-1.64	-1.21	-1.56
	Au	-0.13	0.39	-0.17
3AD @ 111	Co	-2.83	-2.86	-3.01
	Ni	-2.67	-2.51	-2.47
	Cu	-0.92	-1.09	-1.27
	Rh	-2.30	-2.11	-2.27
	Pd	-1.99	-1.41	-1.39
	Ag	0.08	0.23	-0.22
	Ir	-2.92	-2.25	-2.68
	Pt	-2.11	-1.79	-1.86
	Au	-0.30	0.10	-0.30

Table A4. Difference between the adsorption energies of *NHO and *NOH.

facet	metal	$\Delta G^*_{\text{NHO}} - \Delta G^*_{\text{NOH}}$ [eV]
111	Co	0.34
	Ni	0.37
	Cu	0.14
	Rh	0.12
	Pd	0.22
	Ag	-0.30
	Ir	0.12
	Pt	0.26
	Au	-0.30
100	Co	-0.26
	Ni	-0.11
	Cu	-0.21
	Rh	-0.29
	Pd	-0.15
	Ag	-0.24
	Ir	-0.45
	Pt	-0.39
	Au	-0.43
211	Co	-0.06
	Ni	0.15
	Cu	-0.13
	Rh	-0.02
	Pd	0.02
	Ag	-0.51
	Ir	-0.19
	Pt	-0.28
	Au	-0.29

	Co	-0.01
	Ni	0.13
	Cu	-0.22
	Rh	-0.10
211k	Pd	0.10
	Ag	-0.48
	Ir	-0.58
	Pt	-0.10
	Au	-0.48

	Co	-0.49
	Ni	-0.24
	Cu	-0.34
	Rh	-0.51
4AD @ 100	Pd	-0.20
	Ag	-0.38
	Ir	-0.54
	Pt	-0.35
	Au	-0.56

	Co	-0.15
	Ni	0.04
	Cu	-0.18
	Rh	-0.16
3AD @ 111	Pd	0.01
	Ag	-0.45
	Ir	-0.43
	Pt	-0.07
	Au	-0.40

Table A5. Slope and Offset values for each facet for *NOH vs *NO and *NHO vs *NO.

NOH vs NO			
facet	cn	slope	offset [eV]
111	9	1.07	0.16
100	8	1.10	0.15
211	7	1.04	0.30
211k	6	0.95	0.22
4AD @ 100	6	1.00	0.23
3AD @ 111	5	0.95	0.17
	avg	1.02 ± 0.06	0.20 ± 0.06
NHO vs NO			
facet	cn	slope	offset [eV]
111	9	0.83	-0.02
100	8	1.08	-0.16
211	7	0.90	-0.06
211k	6	0.82	-0.18
4AD @ 100	6	1.00	-0.16
3AD @ 111	5	0.87	-0.18
	avg	0.92 ± 0.10	-0.13 ± 0.07

